Electronic Supplementary Material (ESI) for Journal of Materials Chemistry A.

Supplementary Information

to

Porous purple glass – Cobalt imidazolate glasses with accessible porosity from a meltable cobalt imidazolate framework

Louis Frentzel-Beyme,[a] Marvin Kloß,[a] Roman Pallach,[a] Soma Salamon,[b] Henning Moldenhauer,[c] Joachim Landers,[b] Heiko Wende,[b] Jörg Debus,[c] and Sebastian Henke*[a]

[a] Anorganische Chemie, Fakultät für Chemie & Chemische Biology, Technische Universität Dortmund, Otto-Hahn-Straße 6, 44227 Dortmund, Germany.
[b] Fakultät für Physik und Center for Nanointegration Duisburg-Essen (CENIDE), Universität Duisburg-Essen, Lotharstr. 1, 47057 Duisburg, Germany.
[c] Experimentelle Physik 2, Fakultät Physik, Technische Universität Dortmund, Otto-Hahn-Straße 4a, 44227 Dortmund, Germany.

Email: sebastian.henke@tu-dortmund.de

Contents

1 Synthesis and evacuation

All ZIFs were prepared by a modified procedure adapting previously published protocols.[1–4]
In general, $M(NO_3)_2 \cdot 6H_2O$ (4.0 mmol, 1.2 g, $M^{2+} = Zn^{2+}$ or Co^{2+}) and either only imidazol (Him; 0.90 mg, 13.2 mmol) for the ZIF-4(M) compounds or a mixture of 7 eq. imidazole (0.786 g, 11.55 mmol) and 1 eq. benzimidazole (Hbim; 0.196 mg, 1.66 mmol) for the ZIF-62(M) compounds were dissolved in 90 mL *N*,*N*-dimethylformamide (DMF). The obtained solution was divided in ten 9 mL portions, which were transferred into ten 12 mL borosilicate vials. The tightly sealed reaction vials were transferred to a preheated oven (100 °C for the Zn-based compounds, 130 °C for the Co-based compounds) for 7 d. After cooling to room temperature, the reaction volumes were recombined, filtered and washed three times with 20 mL DMF. The ZIFs were obtained as large, truncated octahedrally shaped single crystals (colourless for Zn-ZIFs, deep purple for Co-ZIFs). After characterisation the as-synthesised materials were dried at 200 °C under dynamic vacuum ($p \sim 10^{-3}$ mbar) for 20 h and finely ground using a morat and pestil to obtain the evacuated materials.
For the ZIF-62(M) compounds ^1H NMR spectroscopy was used to determine the im^-:bim^- ratio of the evacuated ZIF crystals (see Table S1).

Table S1. Applied and found im^-:bim^- ratios in the ZIF-61(M) compounds.

Compound	im^-:bim^- (applied)	x [a] (applied)	x [a] (found)
ZIF-62(Zn)	7:1	0.25	0.35
ZIF-62(Co)	7:1	0.25	0.30

[a] $x = 2 \cdot c(bim^-) / (c(im^-) + c(bim^-))$; c = molar concentration in the synthesis solution or the solid.

Note, ZIF-62(Zn) contained a small amount of DMF (~0.04 molecules per formula unit) after the activation process, likely because of the very narrow pore openings due to the slightly larger number of bim^- linkers.

2 X-ray powder diffraction

X-ray powder diffraction (XRPD) patterns were recorded on a Siemens D5005 diffractometer in Bragg-Brentano geometry with CuKα radiation in the range from 5° to 50° 2*θ* with a step size of 0.01° or 0.02°. Finely ground samples were deposited on a glass holder or a single crystal zero background sample holder made of silicon (cut along the (610) plane). Structureless profile fitting (Pawley method[5]) were performed with the TOPAS academic v6 software.

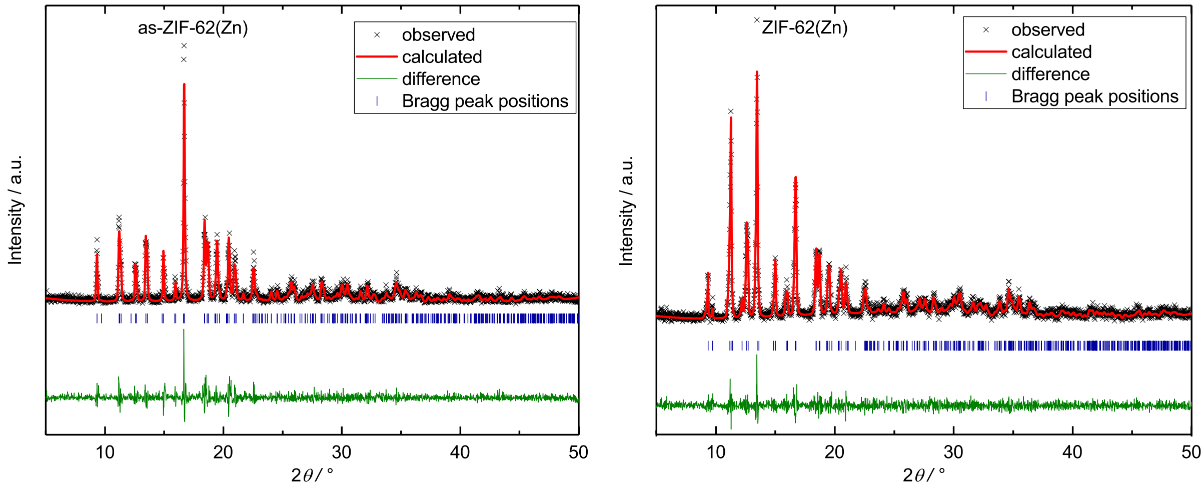

Figure S1. XRPD patterns of ZIF-62(Zn) with Pawley refinements. Left: as-synthesised material containing DMF; Right: dried material without solvent.

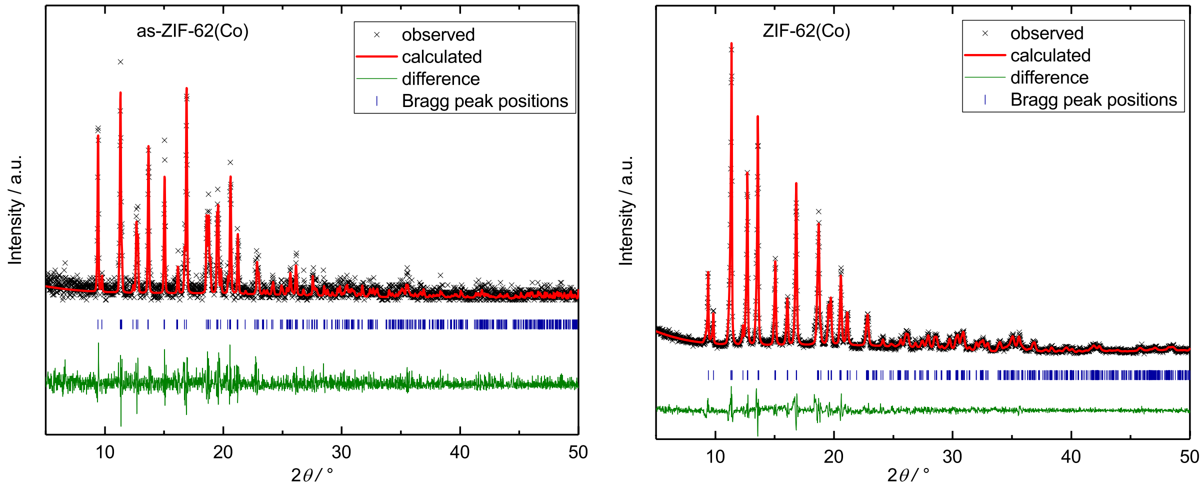

Figure S2. XRPD patterns of ZIF-62(Co) with Pawley refinements. Left: as-synthesised material containing DMF; Right: dried material without solvent.

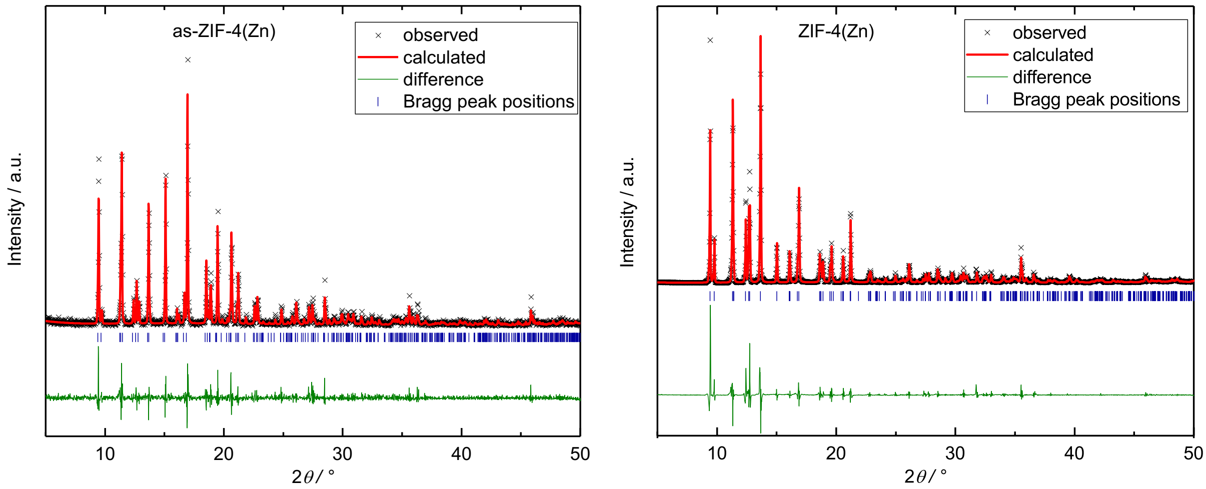

Figure S3. XRPD patterns of ZIF-4(Zn) with Pawley refinements. Left: as-synthesised material containing DMF; Right: dried material without solvent.

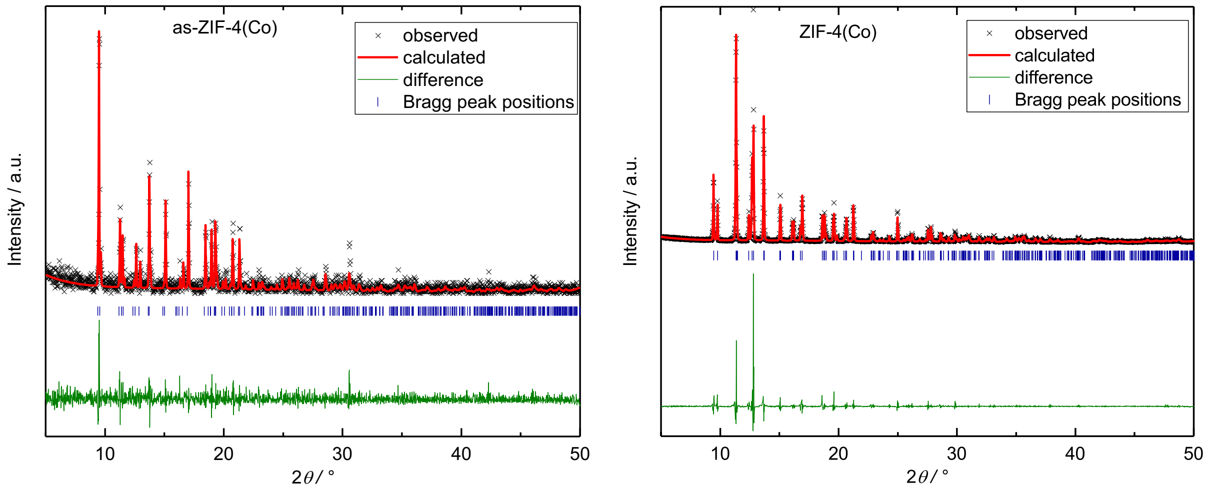

Figure S4. XRPD patterns of ZIF-4(Co) with Pawley refinements. Left: as-synthesised material containing DMF; Right: dried material without solvent.

Table S2. Unit cell parameters *a*, *b*, *c* and *V* (orthorhombic space group *Pbca*) determined by Pawley refinment of the XRPD patterns and the corresponding R_{wp}, R_{exp} and χ values.

Compound	as-ZIF-62(Zn)	ZIF-62(Zn)	as-ZIF-62(Co)	ZIF-62(Co)
a / Å	15.563(7)	15.505(7)	15.477(4)	15.517(3)
b / Å	15.803(8)	15.809(8)	15.551(3)	15.640(2)
c / Å	18.225(8)	18.172(10)	18.152(5)	17.967(3)
V / Å^3	4483(3)	4454(4)	4369.0(19)	4360.4(13)
R_{wp}	30.35	22.26	42.96	11.2
R_{exp}	24.39	19.56	38.83	7.2
χ	1.24	1.14	1.11	1.56

Compound	as-ZIF4(Zn)	ZIF-4(Zn)	as-ZIF-4(Co)	ZIF-4(Co)
a / Å	15.431(2)	15.5205(18)	15.330(5)	15.4180(14)
b / Å	15.627(2)	15.5413(18)	15.549(4)	15.5072(10)
c / Å	18.312(2)	18.108(2)	18.485(5)	18.0832(16)
V / Å^3	4415.9(10)	4367.9(9)	4406(2)	4323.2(6)
R_{wp}	33.71	20.35	46.61	18.06
R_{exp}	26.39	3.09	40.21	6.86
χ	1.27	6.58	1.16	2.63

3 Variable temperature XRPD

Variable temperature XRPD was performed on Beamline BL9 at DELTA (Dortmund, Germany) with a monochromatic X-ray beam (λ = 0.6199 Å) using a MAR345 image plate detector. Finely ground samples were sealed in quartz capillaries, placed on an Anton Paar DHS1100 hot stage and heated under a polyether ether ketone (PEEK) dome. Temperature calibration of the hot stage was performed by reference XRPD measurements of α-quartz.

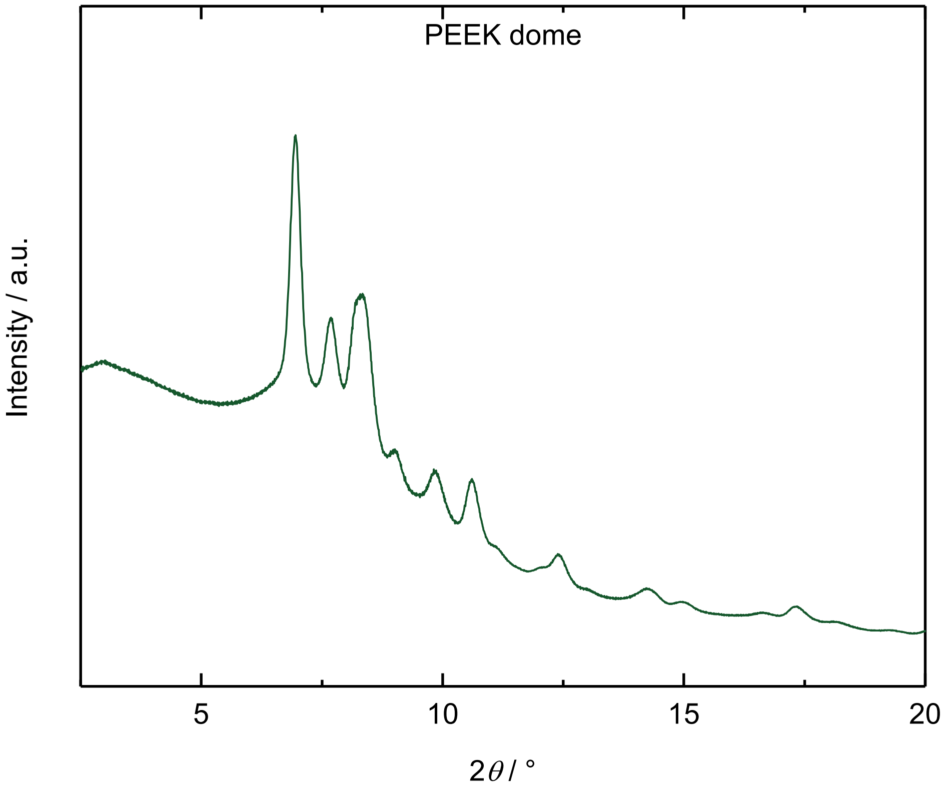

Figure S5. XRPD pattern of the polyether ether ketone (PEEK) dome without sample recorded at 30 °C.

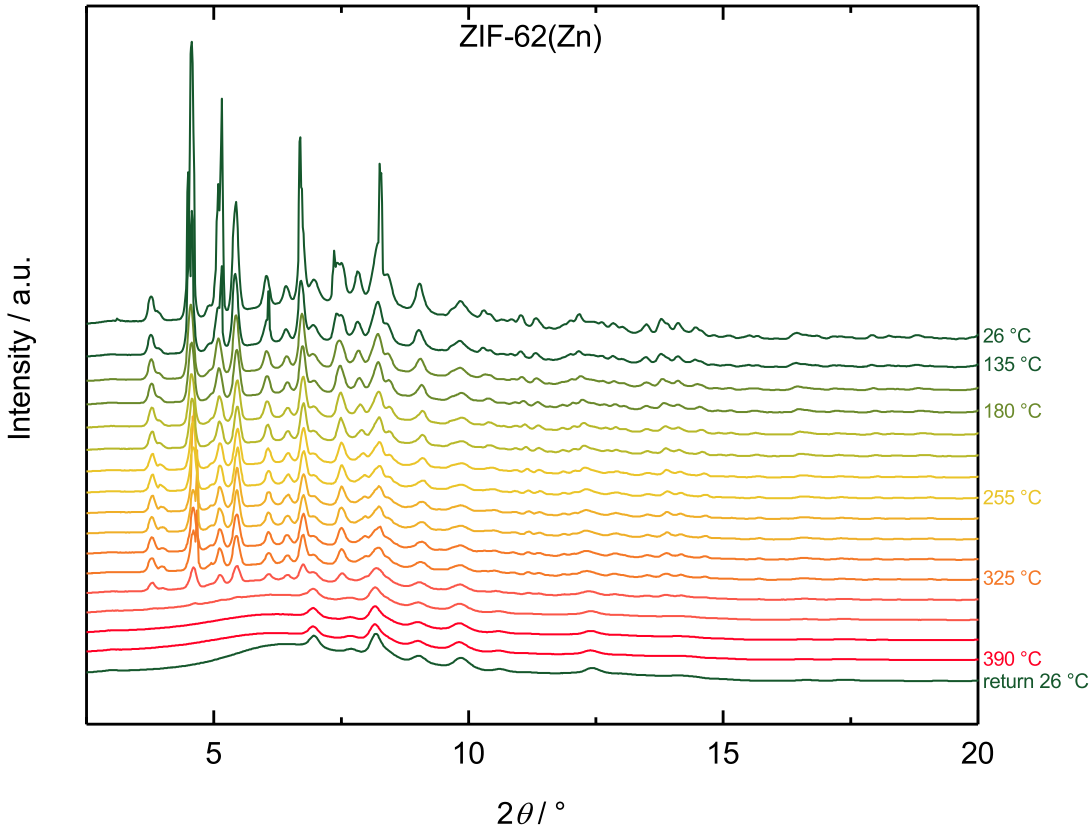

Figure S6. Temperature dependent XRPD patterns of ZIF-62(Zn). The patterns are not normalised but vertically offset for clarity.

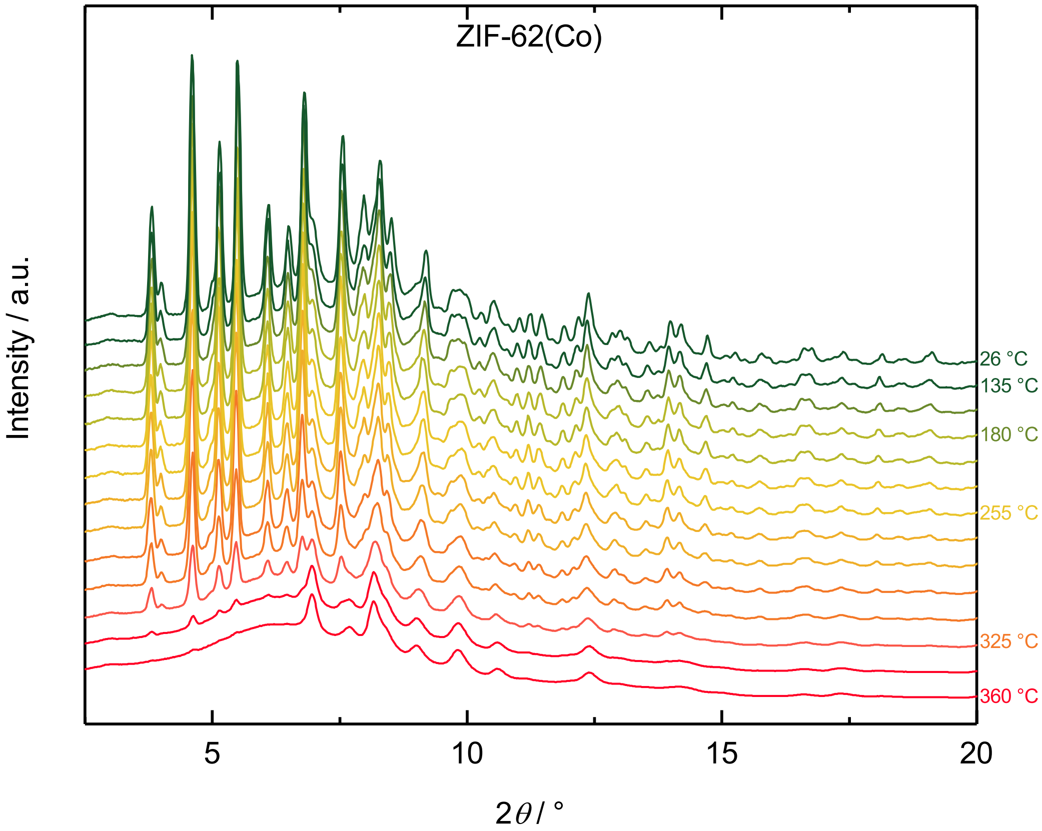

Figure S7. Temperature dependent XRPD patterns of ZIF-62(Co). A pattern after returning to ambient temperature has not been collected because of time constrains. The patterns are not normalised but vertically offset for clarity.

4 Single crystal X-ray diffraction

Single crystal X-ray diffraction data of as-synthesised ZIF crystals were collected on an Oxford Diffraction Xcalibur diffractometer using MoKα radiation. A N_2 cryostream from Oxford Instruments was used for the sample environment (T = 100 K). Data integration, absorption correction and data reduction were performed with the CrysAlisPro software package. Structure solution and refinement were executed with SHELXT and SHELXL[6] using the Olex2[7] interface.

All non-hydrogen atoms were refined anisotropically. Hydrogen atoms were added at geometrical positions and refined isotropically using a riding model. Consistent with previous reports on ZIF-62(Zn) only one crystallographic position for the bim⁻ linker could be resolved in the structures of the as-synthesied ZIF-62(M) materials. The occupancy of these partially occupied bim⁻ linker was set to 50%, because an occupancy higher than 50% would be chemically unreasonable due to steric reasons. According to ^{1}H NMR spectroscopy data, bim⁻ linkers must also partially occupy other positions in the crystal structure of as-ZIF-62(M) because the concentration of bim⁻ is a little higher. However, these locations could not be resolved due to severe disorder.

A number of contraints and restraints were applied for the bim⁻ linker, disordered im⁻ linkers and DMF guest molecules (for the as-ZIF-4(M) compounds). These details are included in the crystallographic information files available from the CSD (see Table S4-S5 for deposition numbers).

The DMF guest molecules could be fully resolved for the as-ZIF-4(M) compounds, however, were severely disordered in the as-ZIF-62(M) crystals. The electron density corresponding to the DMF guests was subtracted from the experimental data by a solvent mask as implemented in Olex2.[7] The number of subtracted electrons corresponds to approx. 0.5 DMF molecules (i.e. 20 e^-) per formula unit.

Table S3. Void volume (V_{void}) and number of electrons (n_e) per void determined by the solvent mask routine of Olex2.[7] Based on the number of electrons the number of DMF molecules (n_{DMF}) per void and per formula unit has been calculated. as-ZIF-62(Zn) contains four voids per unit cell, while as-ZIF-62(Co) contains eight smaller voids.

Compound	V_{void} / Å^3	n_e per void	n_{DMF} per void	n_{DMF} per formula unit
as-ZIF-62(Zn)	305.6	74.3	1.85	0.46
as-ZIF-62(Co)	162.7	35.2	0.88	0.44

Table S4. Crystallographic data of as-ZIF-62(Zn) and as-ZIF-62(Zn).

Compound	as-ZIF-62(Zn)	as-ZIF-62(Co)
CCDC deposition number	1849816	1849817
Empirical formula	$C_7H_{6.5}N_4Zn$	$C_7H_{6.5}CoN_4$
Formula weight / g mol^{-1}	212.03	205.59
Temperature / K	100(2)	100(2)
Crystal system	orthorhombic	orthorhombic
Space group	*Pbca*	*Pbca*
a / Å	15.4567(8)	15.4329(12)
b / Å	15.5793(8)	15.6983(9)
c / Å	18.1340(8)	18.1310(12)
α / Å	90	90
β / Å	90	90
γ / Å	90	90
V / Å^3	4366.7(4)	4392.6(5)
Z	16	16
ρ_{calc} / g cm^{-3}	1.290	1.244
μ / mm^{-1}	2.207	1.520
F(000)	1704.0	1656.0
Crystal size / mm^3	0.351 × 0.291 × 0.173	0.353 × 0.331 × 0.165
Radiation	MoK$_\alpha$ (λ = 0.71073)	MoK$_\alpha$ (λ = 0.71073)
2Θ range for data collection / °	4.338 to 56.992	5.19 to 59.996
Index ranges	$-20 \le h \le 19$, $-20 \le k \le 17$, $-24 \le l \le 12$	$-19 \le h \le 21$, $-22 \le k \le 21$, $-21 \le l \le 25$
Reflections collected	13192	18464
Independent reflections	5327 [R_{int} = 0.0301, R_{sigma} = 0.0439]	6396 [R_{int} = 0.0370, R_{sigma} = 0.0426]
Data/restraints/parameters	5327/39/253	6396/31/253
Goodness-of-fit on F^2	1.020	1.027
Final R indexes [I ≥ 2σ (I)]	R_1 = 0.0512, wR_2 = 0.1267	R_1 = 0.0551, wR_2 = 0.1317
Final R indexes [all data]	R_1 = 0.0772, wR_2 = 0.1411	R_1 = 0.0925, wR_2 = 0.1615
Largest diff. peak/hole / e Å^{-3}	0.93/-0.43	0.63/-0.31

Table S5. Crystallographic data of as-ZIF-4(Zn) and as-ZIF-4(Co)

Compound	as-ZIF-4(Zn)	as-ZIF-4(Co)
CCDC deposition number	1849813	1849807
Empirical formula	$C_{7.5}H_{9.5}N_{4.5}O_{0.5}Zn$	$C_{7.5}H_{9.5}CoN_{4.5}O_{0.5}$
Formula weight / g mol^{-1}	236.07	229.63
Temperature / K	100(2)	103(2)
Crystal system	orthorhombic	orthorhombic
Space group	*Pbca*	*Pbca*
a / Å	15.6595(5)	14.7957(5)
b / Å	14.6464(4)	15.5641(5)
c / Å	18.3890(7)	18.4453(6)
α / Å	90	90
β / Å	90	90
γ / Å	90	90
V / Å^3	4217.6(2)	4247.6(2)
Z	16	16
ρ_{calc} / g cm^{-3}	1.487	1.436
μ / mm^{-1}	2.298	1.585
F(000)	1920.0	1872.0
Crystal size / mm^3	0.575 × 0.435 × 0.372	0.819 × 0.576 × 0.34
Radiation	MoK$_\alpha$ (λ = 0.71073)	MoK$_\alpha$ (λ = 0.71073)
2Θ range for data collection / °	5.138 to 64.848	5.204 to 56.96
Index ranges	$-23 \leq h \leq 22$, $-8 \leq k \leq 20$, $-27 \leq l \leq 23$	$-19 \leq h \leq 14$, $-20 \leq k \leq 20$, $-13 \leq l \leq 24$
Reflections collected	17421	16292
Independent reflections	6905 [R_{int} = 0.0215, R_{sigma} = 0.0267]	5088 [R_{int} = 0.0227, R_{sigma} = 0.0239]
Data/restraints/parameters	6905/0/246	5088/12/246
Goodness-of-fit on F^2	1.032	1.044
Final R indexes [I ≥ 2σ (I)]	R_1 = 0.0282, wR_2 = 0.0715	R_1 = 0.0415, wR_2 = 0.1105
Final R indexes [all data]	R_1 = 0.0369, wR_2 = 0.0756	R_1 = 0.0532, wR_2 = 0.1220
Largest diff. peak/hole / e Å^{-3}	0.93/-0.35	1.22/-1.07

5 X-ray total scattering and pair distribution function analysis

X-ray total scattering data were collected at beamline I15-1 of Diamond Light Source (UK) using a monochromatic X-ray beam (λ = 0.161669 Å, 76.7 keV). Finely ground samples were loaded into 1.5 mm (outer diameter) borosilicate capillaries. Scattering data from an empty capillary were used for background subtraction. Corrections for background, multiple, container and Compton scattering, as well as for absorption were done with the GudrunX program.[8] The X-ray pair distribution functions (XPDFs) in the form of $D(r)$ were obtained via Fourier transform of the normalized reciprocal space data ($S(Q)$).

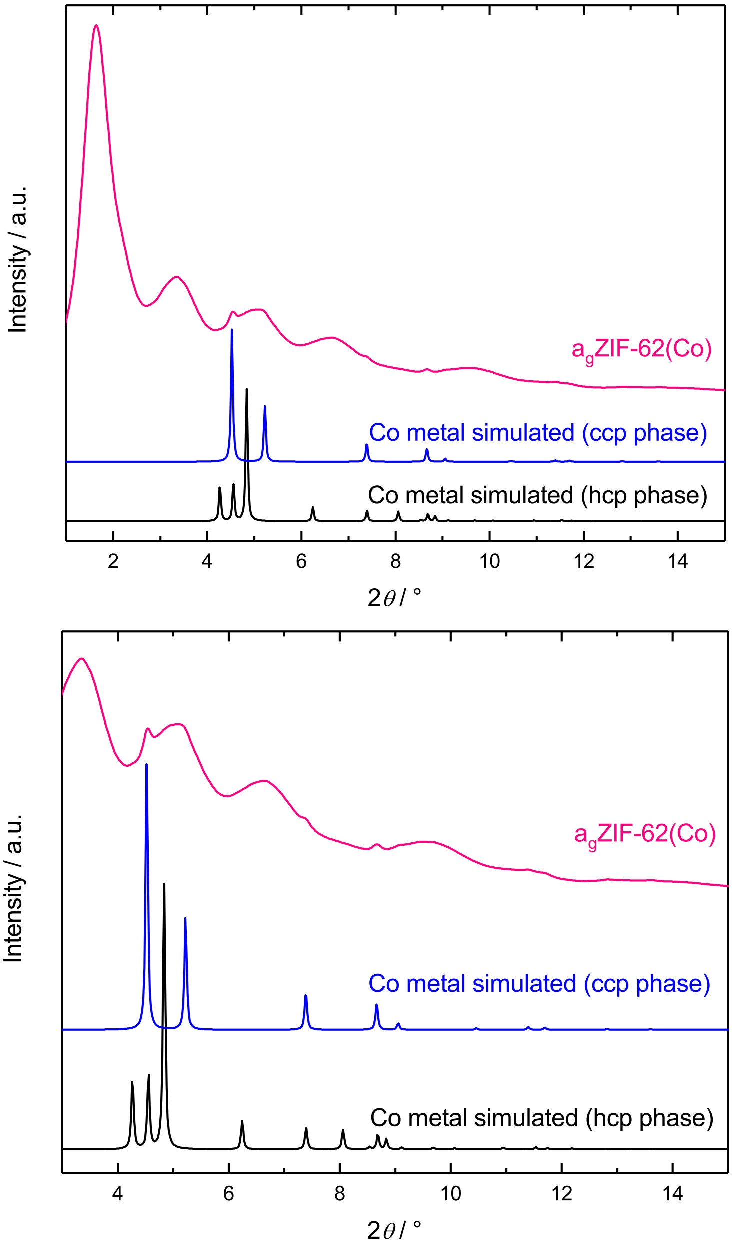

Figure S8. X-ray scattering data of the glass of ZIF-62(Co) collected at beamline I15-1 of Diamond Light Source (λ = 0.161669 Å). Besides the broad diffuse scattering from the ZIF glass, weak Bragg peaks are evident. The crystalline impurity can be identified clearly as Co metal (ccp phase). This is in accordance with magnetic measurements (see main text), which suggest the presence of about 0.82 wt% of Co metal alongside the ZIF glass.

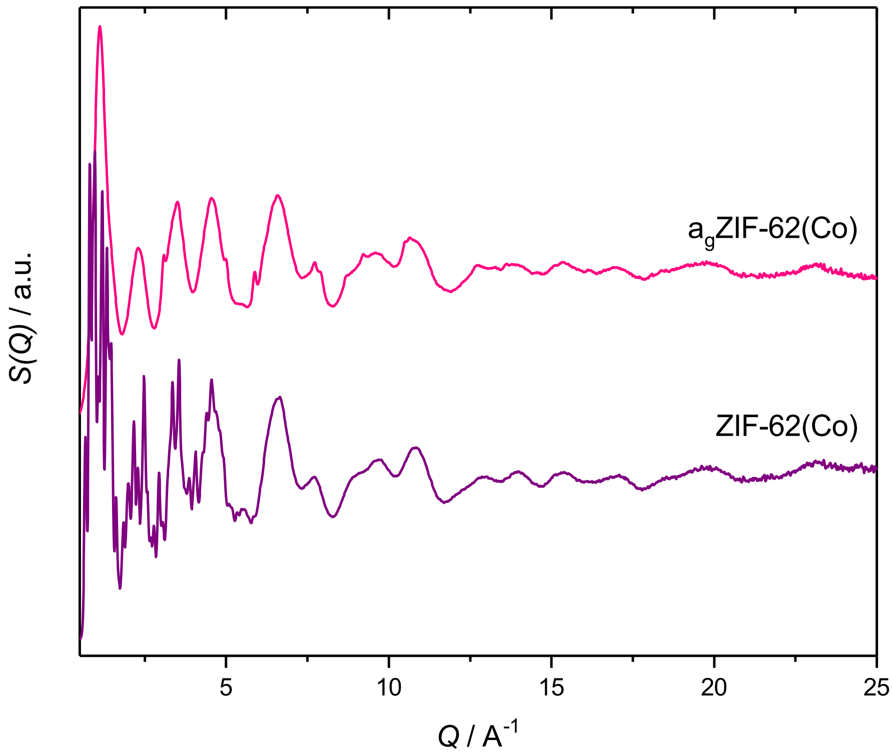

Figure S9. X-ray scattering factors for the crystalline and glass phases of ZIF-62(Co) determined from total scattering data recorded at beamline I15-1 of Diamond Light Source. The weak but sharp features in the *S*(*Q*) of the glass indicate the presence of a minor crystalline impurity, which was identified as Co metal (ccp phase).

6 Thermogravimetric analysis / differential scanning calorimetry

Simultaneous thermogravimetric analysis / differential scanning calorimetry (TGA/DSC) measurements were conducted on a SDT Q600 V5.0 Build 63 instrument (TA instruments, USA) under a constant argon flow (4 L h^{-1}). Two different TGA/DSC programs each with a scan rate of ±10 °C min^{-1} were utilised.

TGA/DSC program 1 (one upscan):
T = 25 °C → 750 °C

TGA/DSC program 2 (three upscans, two downscans):
T = 25 °C → 475 °C → 50 °C → 475 °C → 50 °C → 475 °C

T_m was defined as the offset temperature of the endothermal melting peak and has been determined by the intersection of two tangents. ΔH_m is the integral area between the onset and offset of the melting peak in the DSC curve. ΔS_m was calculated as $\Delta H_\mathrm{m}/T_\mathrm{m}$. The glass transition temperatur (T_g) was determined based on the data obtained via TGA/DSC program 2. The onset of the endothermal glass transition peak in the DSC curve (second upscan) was determined by the intersection of two tangents. None of the downscans (program 2) showed any thermal features, i.e. endothermic peaks corresponding to a recrystalisation of the melted/glassy ZIF.

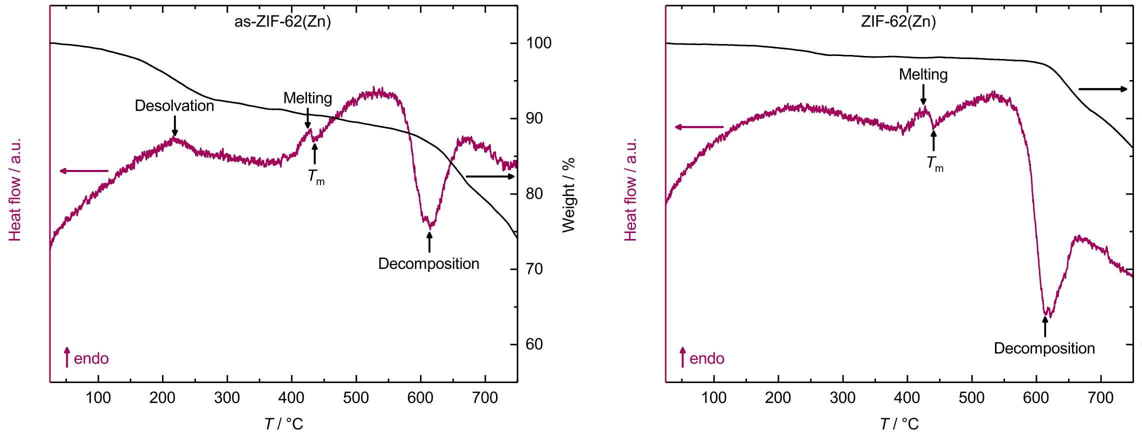

Figure S10. TGA/DSC data of the as-synthesised ZIF-62(Zn) (left) and the desolvated sample (right) using TGA/DSC program 1.

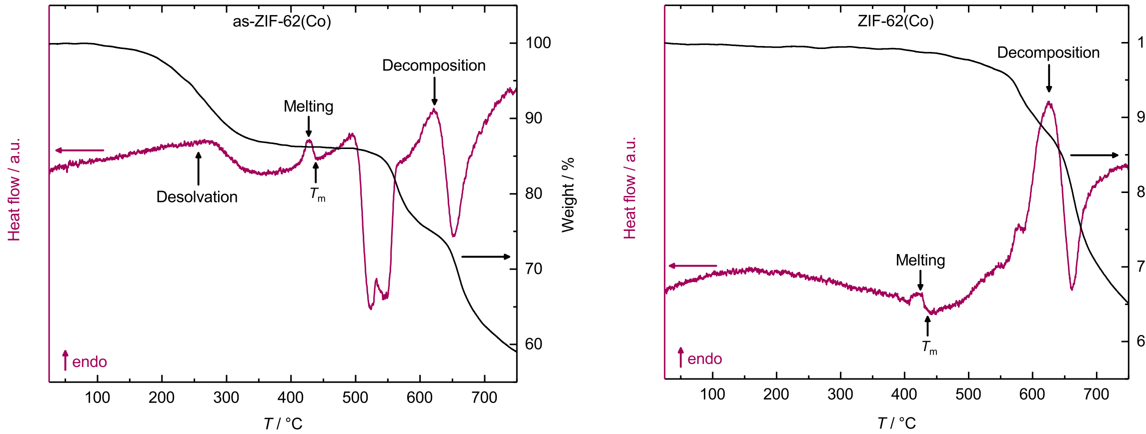

Figure S11. TGA/DSC data of the as-synthesised ZIF-62(Co) (left) and the desolvated sample (right) using TGA/DSC program 1.

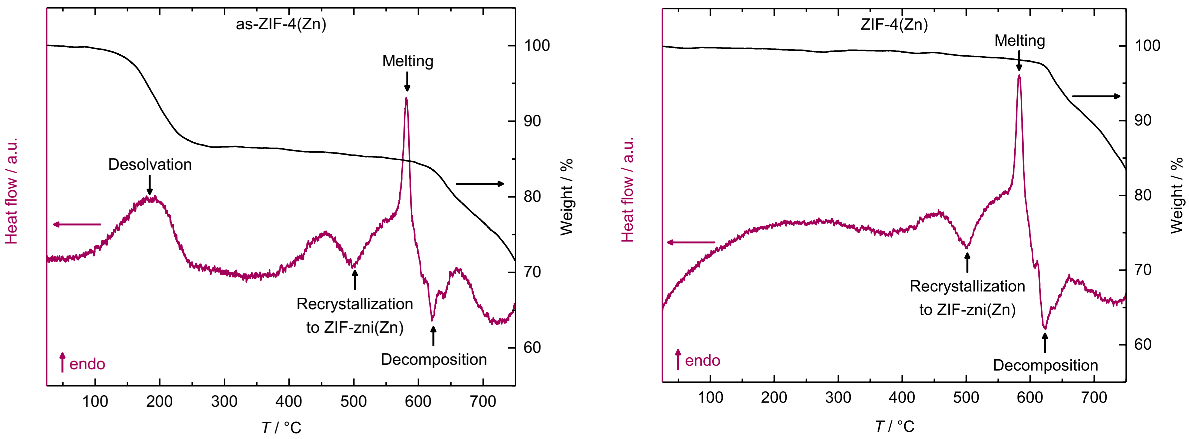

Figure S12. TGA/DSC data of the as-synthesised ZIF-4(Zn) (left) and the desolvated sample (right) using TGA/DSC program 1.

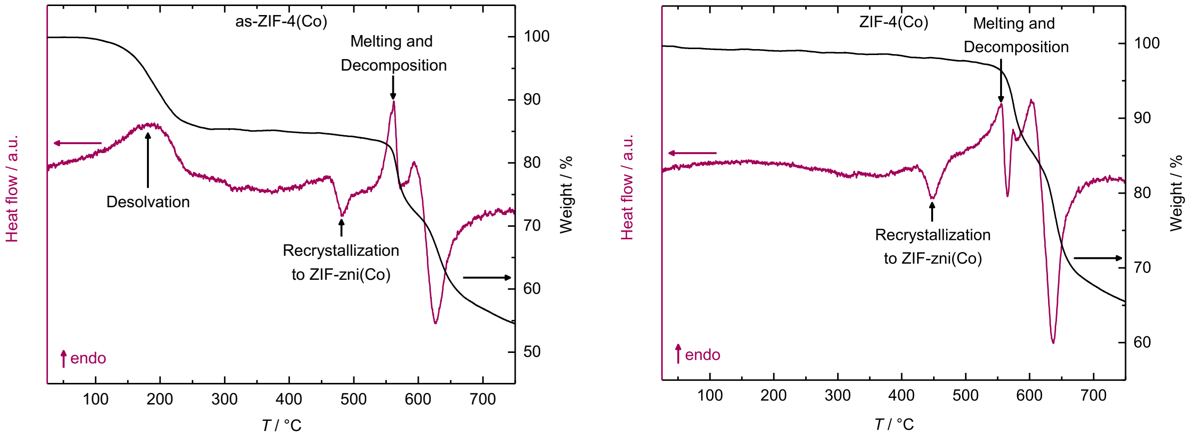

Figure S13. TGA/DSC data of the as-synthesised ZIF-4(Co) (left) and the desolvated sample (right) using TGA/DSC program 1.

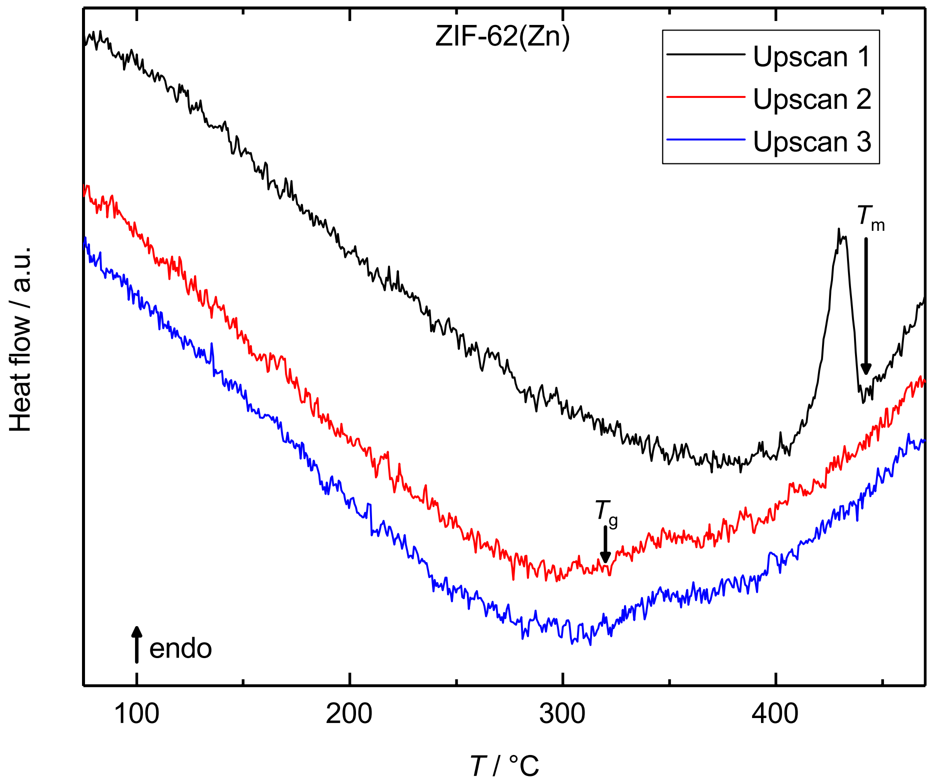

Figure S14. DSC data of ZIF-62(Zn) using TGA/DSC program 2.

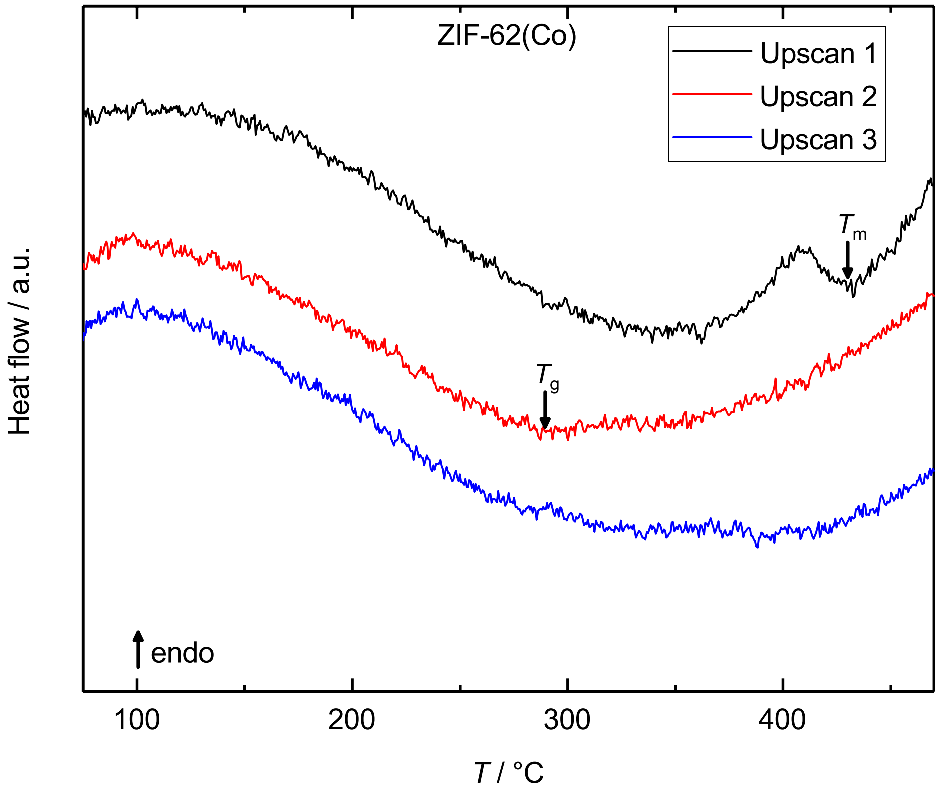

Figure S15. DSC data of ZIF-62(Co) using TGA/DSC program 2.

Table S6. Thermodynamic data of the ZIF-62(M) compounds. The data have been extracted from TGA/DSC curves recorded with program 2.

Compound	T_m / °C	ΔH_m / kJ mol^{-1}	ΔS_m / J mol^{-1} K^{-1}	T_g / °C	T_g T_m^{-1} #
ZIF-62(Zn)	441	2.46	3.44	320	0.83
ZIF-62(Co)	432	2.64	3.75	290	0.80

absolute temperatures in K were used

The T_g/T_m ratio is a measure for the glass forming ability of a material.[9] A material with high glass forming ability resists recrystallisation on laboratory time scales. The T_g/T_m ratios of ZIF-62(Co) is very large, signifying its ultrahigh glass forming ability, similar to the current record holder ZIF-62(Zn).

7 Photographs

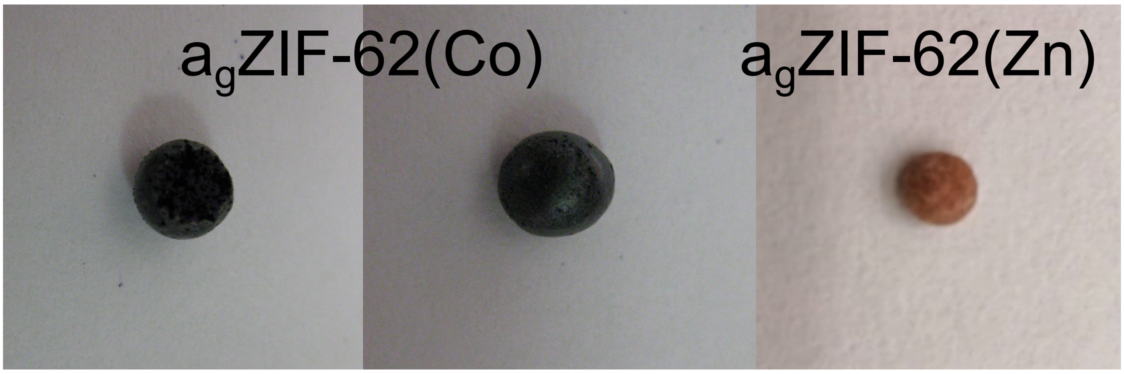

Figure S16. Photographs of the vitrious products obtained after conducting TGA/DSC program 2. Fusion of the finely ground ZIF microparticles into a ZIF glass monolith as a consequence of melting is clearly evident.

8 Infrared spectroscopy

FT-Infrared (IR) spectroscopy was carried out on a Perkin Elmer SpectrumTwo FT-IR spectrometer ($\tilde{\nu}$ = 400 cm^{-1} - 4000 cm^{-1}) in reflection mode using a diamond ATR (attenuated total reflectance) unit. Spectra were collected of the crystalline samples in their as-synthesised and desolvated state as well as on the corresponding glass samples obtained by conducting TGA/DSC program 2 (see Section 6).

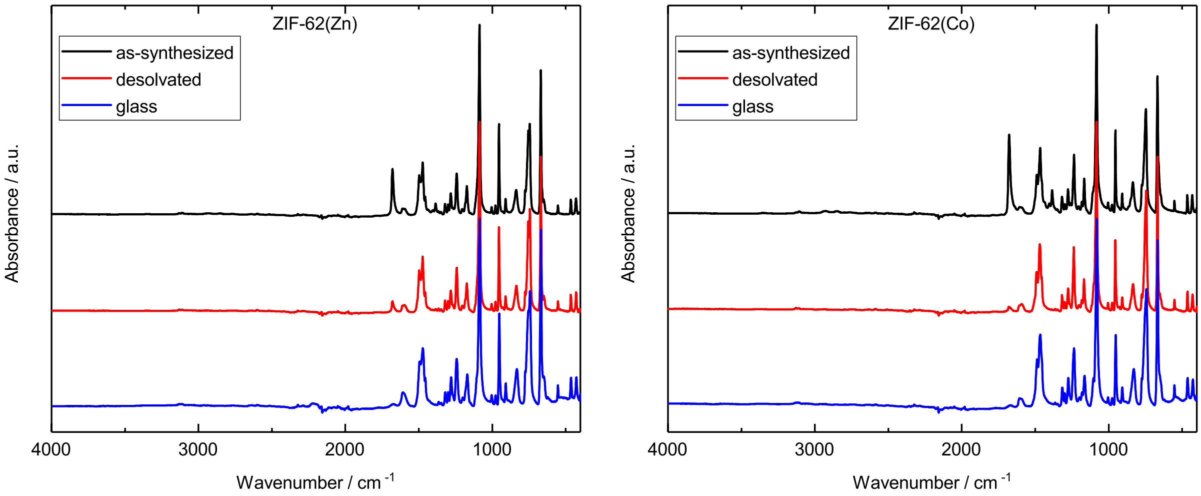

Figure S17. FT-IR spectra of the as-synthesised and desolvated crystalline materials as well as of their corresponding glasses of ZIF-62(M).

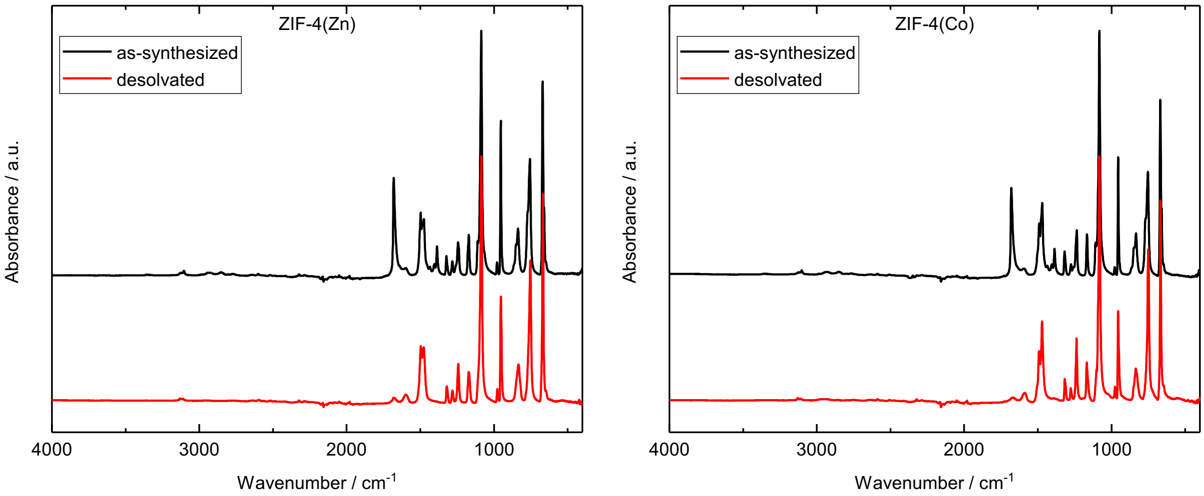

Figure S18. FT-IR spectra of the as-synthesised and desolvated compounds of ZIF-4(M).

9 Raman scattering

Raman scattering measurements were performed with a confocal Raman spectrometer (S&I MonoVista Raman Microscope System CRS+ 750/BX51) providing a spatial resolution of about one micrometer. A Helium-Neon laser with 633 nm excitation wavelength or the fundamental mode of a Nd:YAG single-frequency laser with 1064 nm wavelength was used in the experiments. The laser power was set through neutral density filters and was carefully chosen in order to avoid a degradation of the sample. For that purpose, after each measurement the surface was visually checked using white light illumination and a video camera installed at the microscope. The laser beam was focused with a 50x microscope objective, properly chosen for the respective excitation wavelength used, on the sample. The laser spot size did not exceed 2 μm. The scattered light was examined using a 0.75 m spectrometer (Acton SpectraPro SP2750) with a liquid-nitrogen cooled charge-coupled-device (CCD) camera (Princeton Instruments PyLoN 2KF). For the spectra measured at 633 nm (1064 nm) laser excitation, a Si-based (InGaAs-based) CCD camera was used. Wavelength-adapted edge filters suppressed the laser light, so that scattered light signals with energy shifts of 70 cm^{-1} with respect to the laser line position at zero energy shift could be resolved. The samples were placed on a microscopy table, whose position could automatically be changed with sub-micrometer spatial scanning resolution.

10 ^{1}H NMR spectroscopy

^{1}H NMR spectra of digested ZIF-62(M) samples (crystalline and glass) have been recorded on Bruker DPX-300, DPX 500 or Agilent DD2 500 spectrometers using DMSO-*d*$_6$ (0.5 mL) and DCl/D$_2$O (35 wt%, < 0.1 mL) as solvents. The data were processed with the ACD/Labs software. Data were referenced to the residual proton signal of DMSO and chemical shifts are given relative to tetramethylsilane.

We found a small contamination with a chemical shift of 1.25 ppm in the DCl/D$_2$O solvent. This contamination, however, does not interfere with the data analysis.

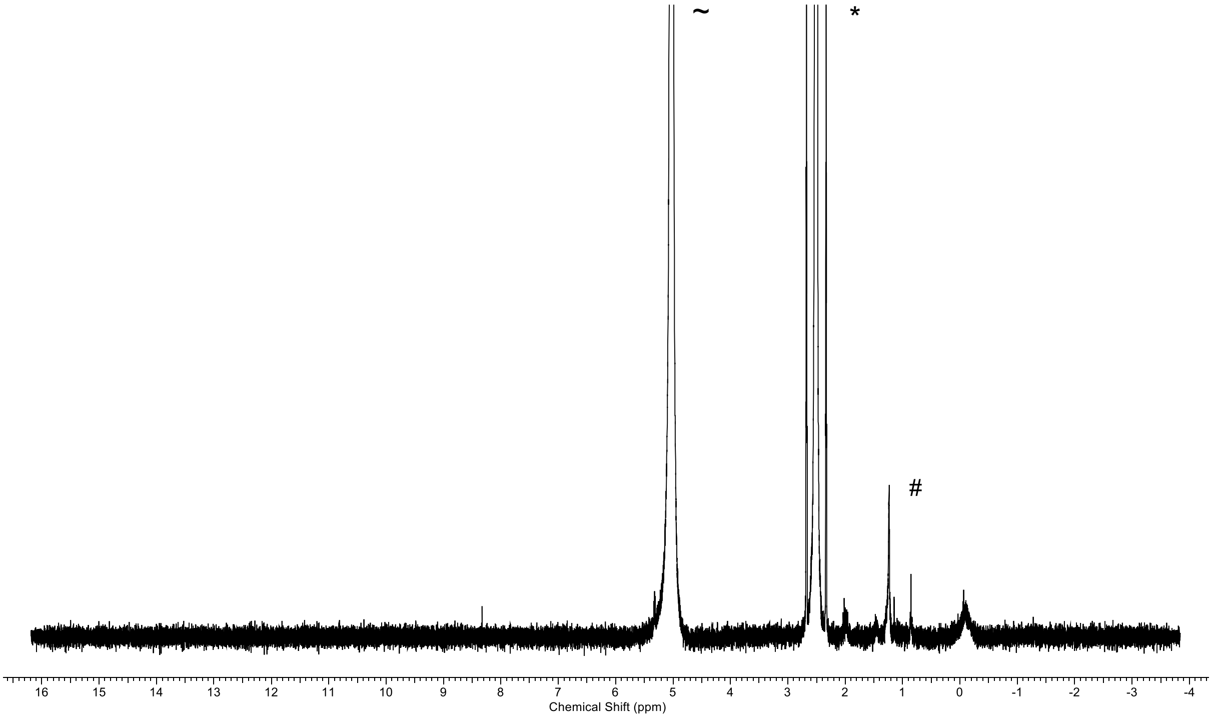

Figure S19. Zoom into the complete ^{1}H NMR spectrum of the DMSO solvent with a drop of DCl/D$_2$O that shows a small, unidentified contamination at 1.25 ppm (marked with #). DMSO is marked with *, D$_2$O is marked with ~.

To determine the amount of bim$^-$ linker in the framework materials the singlet signals of the CH-group (**1a** for im$^-$ linker, **1b** for bim$^-$ linker) between the nitrogen atoms were used to bypass signal overlap. The chemical shift of the signals varies with the concentration of DCl in the solvent. All signals were integrated and the combined singlet signals set to a value of two protons, so that the integral of the signal **1b** corresponds to the amount (x) of bim$^-$ according to the chemical compositon M(im)$_{2-x}$(bim)$_x$.

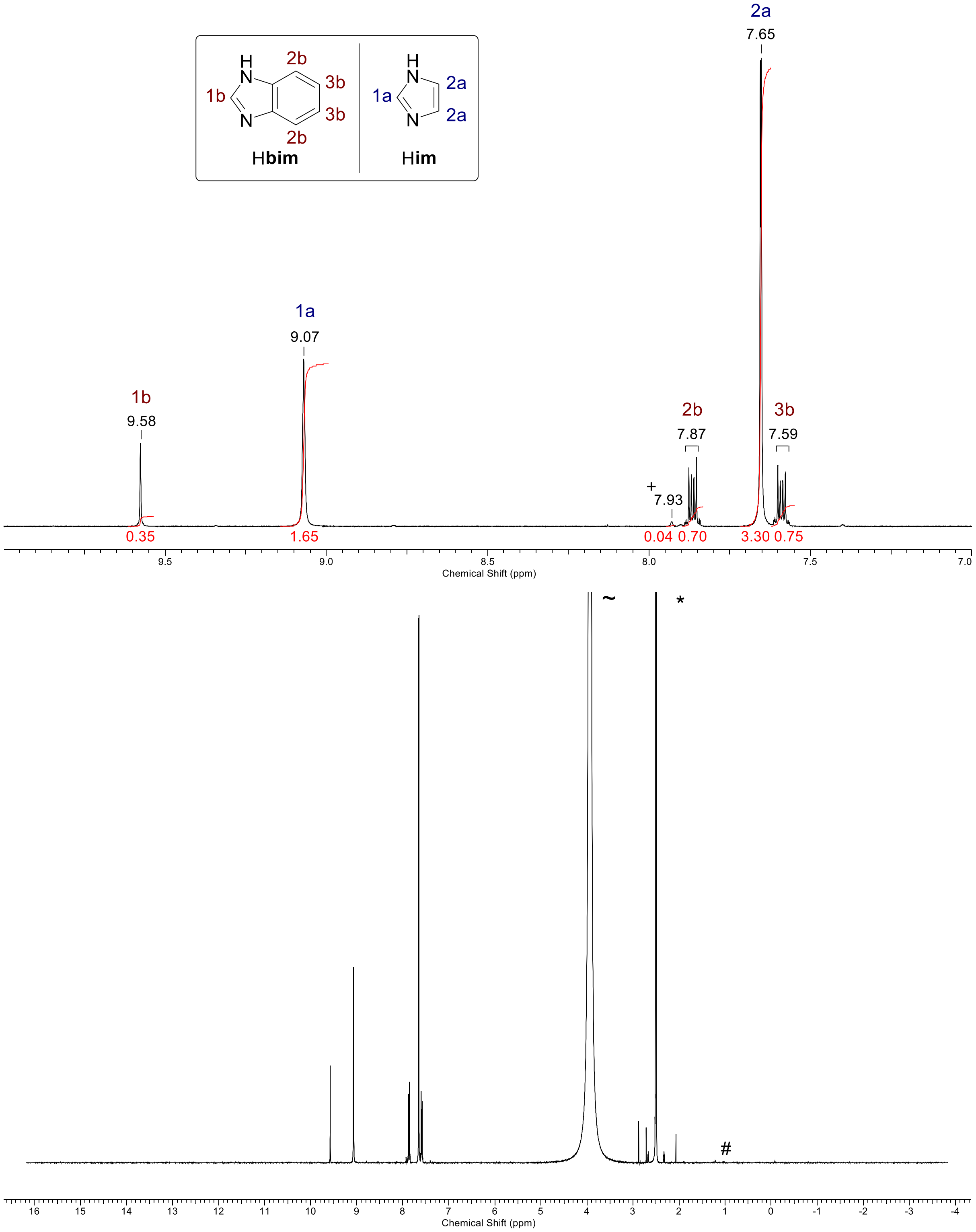

Figure S20. ^{1}H NMR spectrum of a digested sample of ZIF-62(Zn). Top: Zoom in the aromatic region (7.0 to 10.0 ppm). Bottom: Complete spectrum. A very small amount of ~0.04 DMF molecules per formula unit is detected (formyl proton at 7.93 ppm, marked with +). DMSO is marked with *, D_2O is marked with ~ and the small contamination of the DCl/D_2O mixture is marked with #.

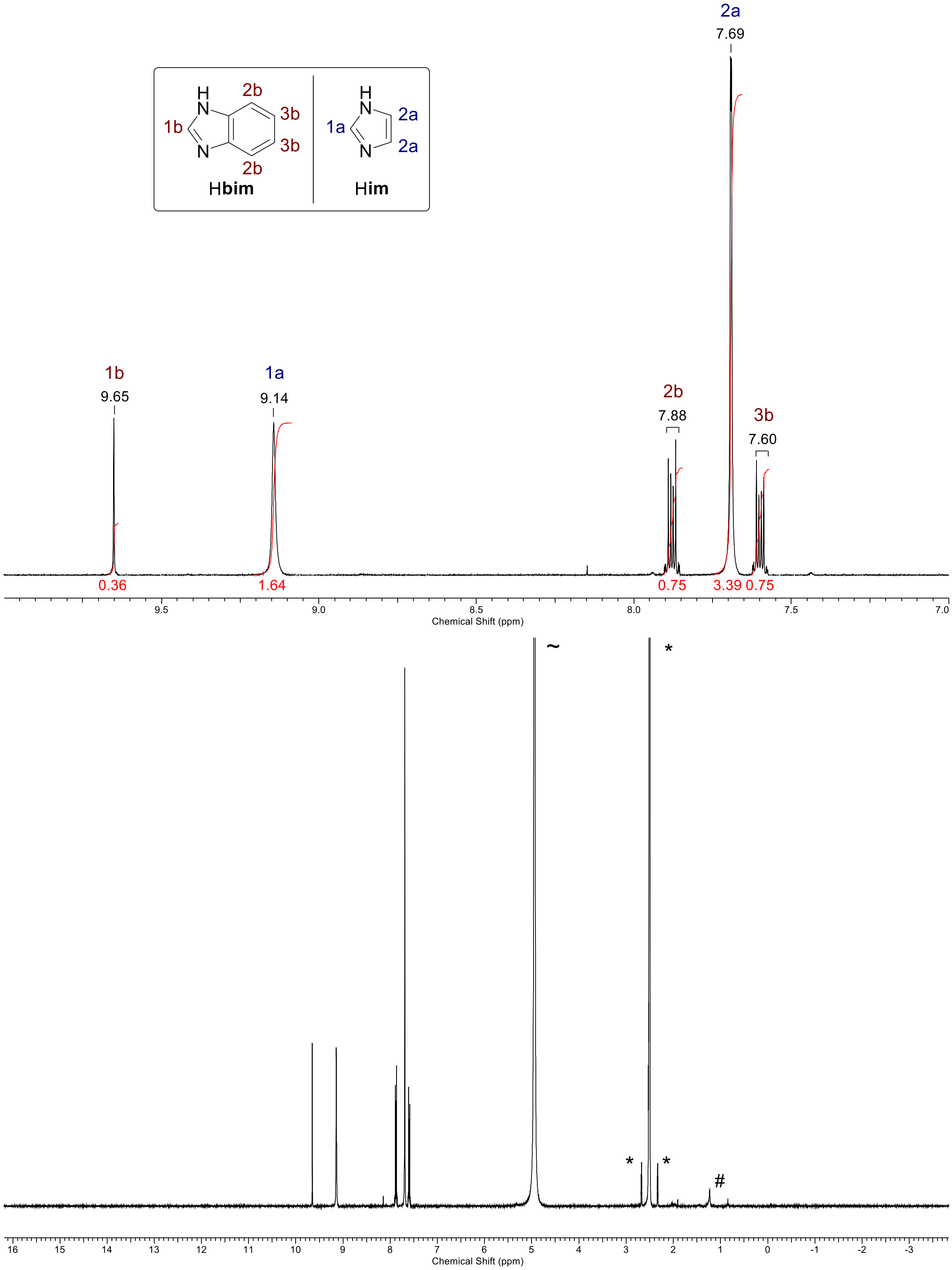

Figure S21. ^{1}H NMR spectrum of a digested sample of a_gZIF-62(Zn). Top: Zoom in the aromatic region (7.0 to 10.0 ppm). Bottom: Complete spectrum. DMSO is marked with *, D_2O is marked with ~ and the small contamination of the DCl/D_2O mixture is marked with #.

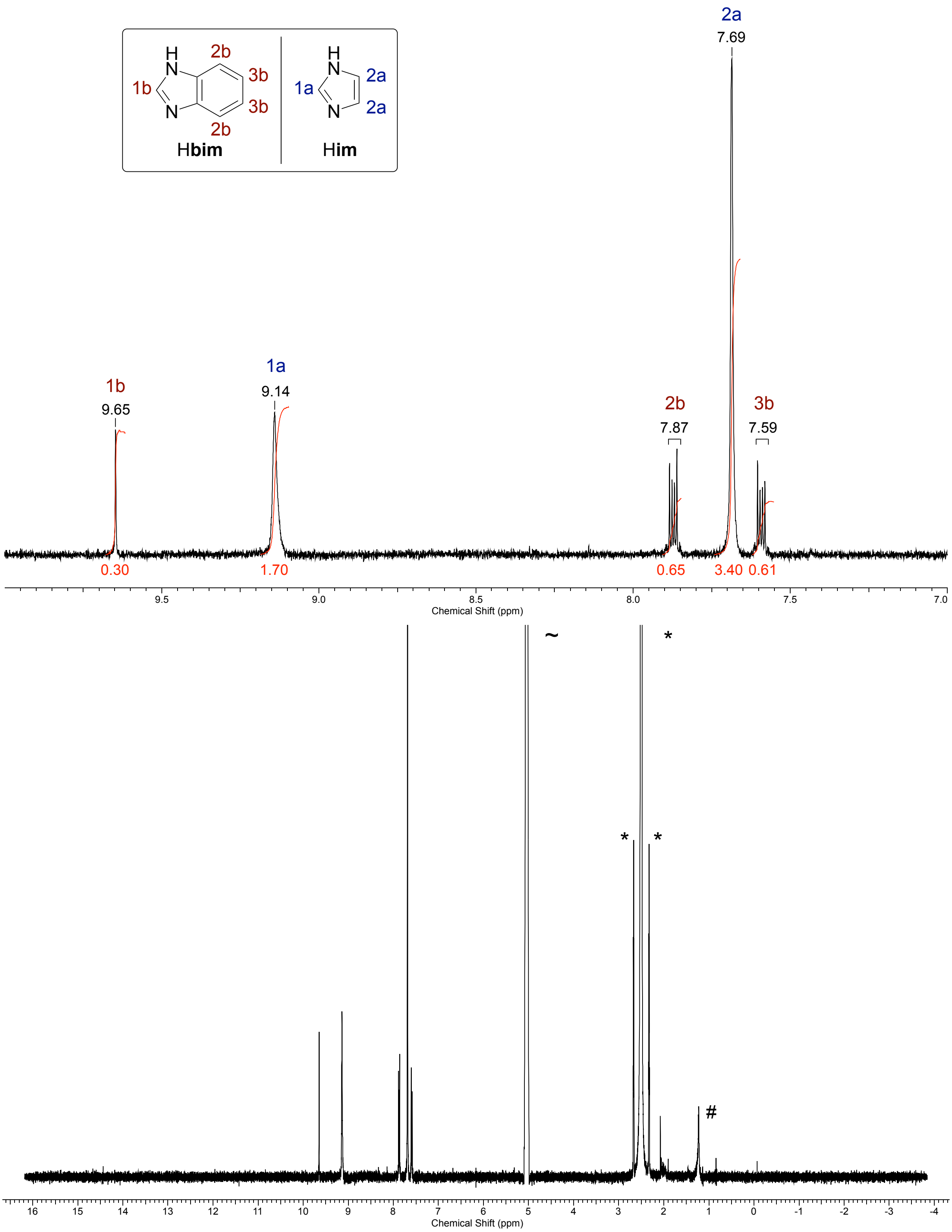

Figure S22. ^1H NMR spectrum of a digested sample of ZIF-62(Co). Top: Zoom in the aromatic region (7.0 to 10.0 ppm). Bottom: Complete spectrum. DMSO is marked with *, D_2O is marked with ~ and the small contamination of the DCl/D_2O mixture is marked with #.

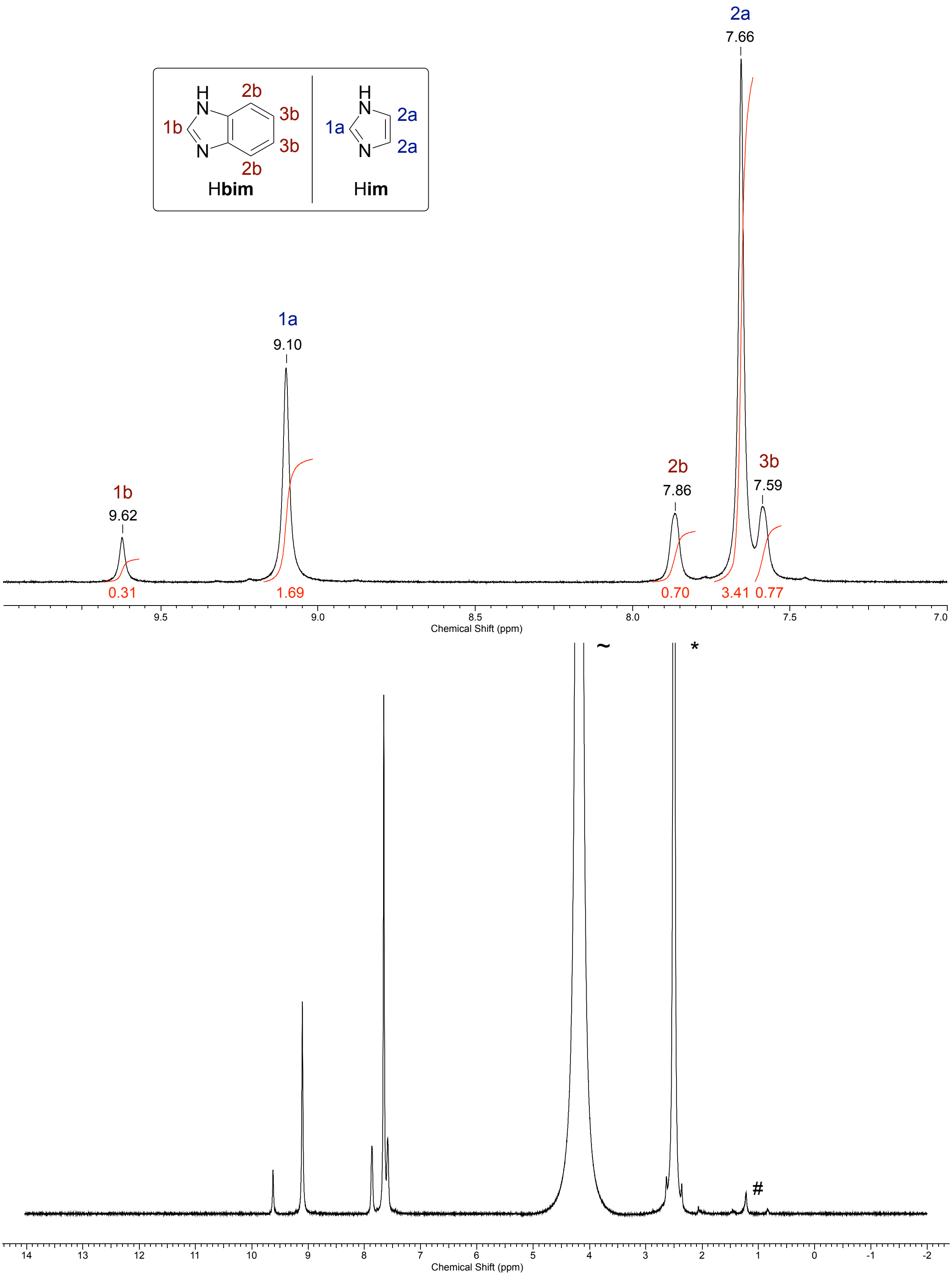

Figure S23. ^{1}H NMR spectrum of a digested sample of a$_g$ZIF-62(Co). Top: Zoom in the aromatic region (7.0 to 10.0 ppm). Bottom: Complete spectrum. DMSO is marked with *, D_2O is marked with ~ and the small contamination of the DCl/D_2O mixture is marked with #.

11 Magnetic measurements

Magnetic measurements as a function of temperature were performed with a Quantum Design MPMS-5S equipped with an AC susceptometry option, while field dependent curves were recorded with the vibrating sample magnetometer (VSM) option of a Quantum Design PPMS DynaCool.

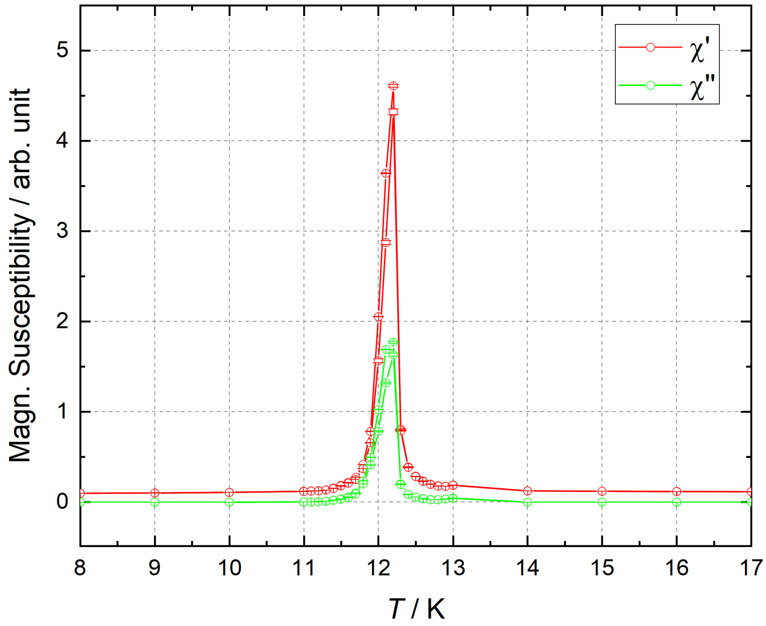

Figure S24. Magnetic AC susceptibility of crystalline ZIF-62(Co) measured at 8 Hz with a field amplitude of 0.4 mT with both rising and falling temperature across the phase transition, which could be determined to be at 12.2(1) K in agreement with temperature dependent magnetometry measurements (see Figure 6).

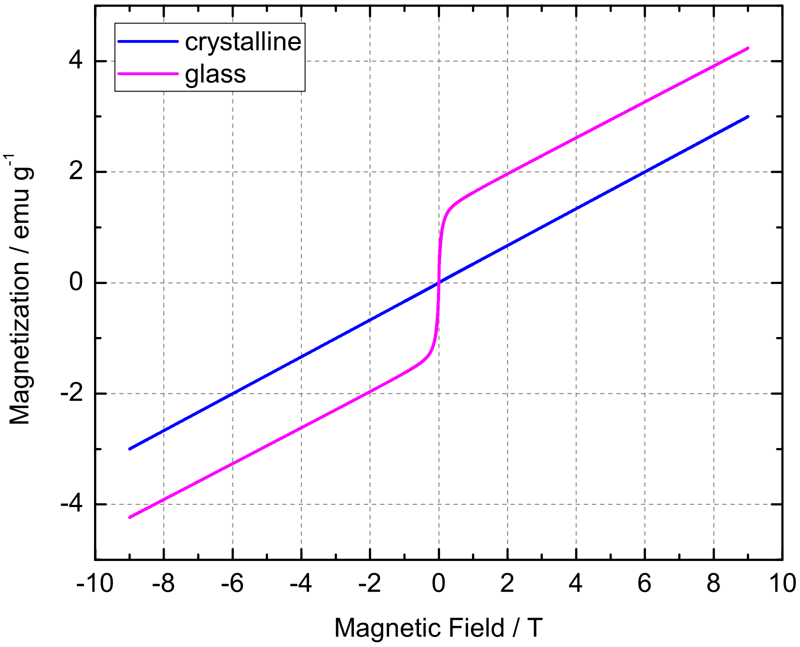

Figure S25. Magnetic field dependent measurements on both crystalline and glass samples of ZIF-62(Co), recorded at 300 K up to ±9 T, showing a purely paramagnetic behavior of the crystalline material. The glass sample shows a small spontaneous magnetization, determined from the linear extrapolation of the high field region (1-9 T) to ca. 1.32 emu/g. X-ray total scattering data reveal the presence of a small amount of metallic cobalt in the glass sample. Assigning the magnetic phase to metallic cobalt with a saturation magnetization of 161 emu/g at room temperature[10], the amount of metallic cobalt in the a_gZIF-62(Co) sample corresponds to 0.82 wt%.

12 Gas sorption

CO_2 gas physisorption measurements were recorded at 273 K with a Quantachrome iQ MP instrument using CO_2 gas of 99.995% purity. A thermostat was used for the sample environment. Samples have been evacuated at high vacuum (turbo molecular pump) and 200 °C for at least one hour prior to data collection.

References

1 M. T. Wharmby, S. Henke, T. D. Bennett, S. R. Bajpe, I. Schwedler, S. P. Thompson, F. Gozzo, P. Simoncic, C. Mellot-Draznieks, H. Tao, Y. Yue and A. K. Cheetham, *Angew. Chem. Int. Ed.*, 2015, **54**, 6447–6451.

2 S. Henke, M. T. Wharmby, G. Kieslich, I. Hante, A. Schneemann, Y. Wu, D. Daisenberger and A. K. Cheetham, *Chem. Sci.*, 2018, **9**, 1654–1660.

3 M. R. Ryder, B. Civalleri, T. Bennett, S. Henke, S. Rudić, G. Cinque, F. Fernandez-Alonso and J. C. Tan, *Phys. Rev. Lett.*, 2014, **113**, 215502.

4 M. Gustafsson and X. Zou, *J. Porous Mater.*, 2013, **20**, 55–63.

5 G. S. Pawley, *J. Appl. Cryst.*, 1981, **14**, 357–361.

6 G. M. Sheldrick, *Acta Cryst.*, 2015, **C71**, 3–8.

7 O. V. Dolomanov, L. J. Bourhis, R. J. Gildea, J. A. K. Howard and H. Puschmann, *J. Appl. Cryst.*, 2009, **42**, 339–341.

8 A. K. Soper and E. R. Barney, *J. Appl. Cryst.*, 2011, **44**, 714–726.

9 A. Qiao, T. D. Bennett, H. Tao, A. Krajnc, G. Mali, C. M. Doherty, A. W. Thornton, J. C. Mauro, G. N. Greaves and Y. Yue, *Sci. Adv.*, 2018, **4**, eaao6827.

10 R. C. Weast, *Handbook of Chemistry and Physics*, CRC Press, 61st edn., 1981.